Weakly nonlinear analysis of viscous dissipation thermal instability in plane Poiseuille and plane Couette flows

Weakly nonlinear analysis of viscous dissipation thermal instability in plane Poiseuille and plane Couette flows

Y. Requilé[1], S. C. Hirata[1], M. N. Ouarzazi[1]† and A. Barletta [2]

[1]Unité de Mécanique de Lille, EA 7512, Université de Lille, Bd. Paul Langevin, 59655 Villeneuve d'Ascq Cedex, France

[2]Department of Industrial Engineering, Alma Mater Studiorum Università di Bologna, Viale Risorgimento 2, Bologna 40136, Italy

(Received xx; revised xx; accepted xx)

The weakly nonlinear stability analysis of plane Poiseuille flow (PPF) and plane Couette flow (PCF) when viscous dissipation is taken into account is considered. The impermeable lower boundary is considered adiabatic, while the impermeable upper boundary is isothermal. The linear stability of this problem has been performed by Barletta and Nield [J. Fluid Mech., **662**, 475-492, (2010)] for PCF and by Barletta et al. [J. Fluid Mech., **681**, 499-514, (2011)] for PPF. These authors found that longitudinal rolls are the preferred mode of convection and the onset of instability is described through the governing parameters $\Lambda = Ge\ Pe^2$ and Pr, where Ge, Pe and Pr are respectively the Gebhart number, the Péclet number and the Prandtl number. The current study focuses on the near-threshold behavior of longitudinal rolls by using a weakly nonlinear analysis. We determine numerically up to third order the coefficients of the Landau amplitude equation and investigate in detail the influences on bifurcation characteristics of the different nonlinearities present in the system. The results indicate that for both PPF and PCF configurations (i) the inertial terms have no influence on the nonlinear evolution of the disturbance amplitude (ii) the nonlinear thermal advection terms act in favour of pitchfork supercritical bifurcations and (iii) the nonlinearities associated to viscous dissipation promote subcritical bifurcations. The global impact of the different nonlinear contributions indicate that independently of Gebhart number the bifurcation is subcritical if $Pr < 0.25$ ($Pr < 0.77$) for PPF (PCF). Otherwise, for higher Prandtl number, there exists a particular value of Gebhart number, Ge^* such that the bifurcation is supercrtical (subcritical) if $Ge < Ge^*$ ($Ge > Ge^*$). Finally, for both PPF and PCF, the amplitude analysis indicates that in the supercritical bifurcation regime, the equilibrium amplitude decreases on increasing Pr and a substantial enhancement (reduction) in heat transfer rate is found for small Pr (moderate or large Pr).

1. Introduction

The purpose of this study is to present a comprehensive account of the nonlinear stability analysis of plane Poiseuille and plane Couette flows in the presence of an unstable temperature gradient. In contrast to the well known Rayleigh-Bénard-Poiseuille and Rayleigh-Bénard-Couette systems where the temprature gradient stems from the externally imposed thermal boundary conditions, here the temperature gradient is induced by viscous dissipation which acts as an internal heat generation.

In the absence of a thermal gradient, plane Poiseuille and plane Couette isothermal

† Email address for correspondence: mohamed-najib.ouarzazi@univ-lille.fr

flows have been extensively investigated in the past as prototype of shear flows. Their linear and nonlinear behaviors are driven purely by inertia, the impact of which can be measured with a single dimensionless parameter, the Reynolds number Re. In summary, Orszag (1971) showed that the plane Poiseuille flow becomes linearly unstable at $Re = 5772$ (Re is based on the channel half-width and the centerline velocity). In the case of weak disturbances in a channel of finite length, the linear threshold $Re = 5772$ was confirmed qualitatively by the experiments conducted by Nishioka *et al.* (1975). For high intensity disturbances in the inlet flow, Nishioka & Asai (1985) concluded from their experiments that the minimum transition Reynolds number is about $Re = 1000$. Numerical simulations performed by Orszag & Patera (1980) showed that finite-amplitude two-dimensional waves become unstable to infinitesimally small three-dimensional perturbations for $Re > 1000$. In the case of plane Couette flow, Romanov (1973) showed that this flow is linearly stable for all Reynolds numbers. In numerical simulations (Dauchot & Daviaud (1995)) and laboratory experiments (Tillmarki & Alfredsson (1992)), the lowest Reynolds numbers at which turbulence can be sustained has been shown to be between 300 and 400.

On the other hand, a vast literature exists on Rayleigh-Bénard-Poiseuille/Couette systems and the interested reader is referred to Nicolas (2002) for a comprehensive review. These systems have recently attracted an increased interest as simple configurations representing open systems to study the transition from convective to absolute instability in Newtonian fluids (Carrière & Monkewitz (1999), D. Martinand & Monkewitz (2006), Ouarzazi *et al.* (2008)), in binary fluid mixtures (Hu *et al.* (2007)) and in viscoelastic fluids (Hirata *et al.* (2015), de B. Alves *et al.* (2016)). Transient growth mechanisms have also been investigated in Rayleigh-Bénard-Poiseuille system by Biau & Bottaro (2004) in the case of a stable stratification. In the presence of unstable stratification due to buoyancy forces, transient growth was analyzed in Rayleigh-Bénard-Poiseuille/Couette systems by Jerome *et al.* (2012).

In the above brief review, the Poiseille/Couette flows are considered isothermal or subjected to external temperature gradient. Recent studies have shown that viscous dissipation can induce thermoconvective instabilities even without external forcing. A bibliographic survey on thermal instabilities induced by viscous dissipation, either in a fluid or in a fluid-saturated porous medium, can be found in Barletta (2015). The buoyancy-induced instability caused by viscous dissipation in plane Couette flow (PCF) and plane Poiseuille flow (PPF) were studied respectively by Barletta & Nield (2010) and Barletta *et al.* (2011). The authors considered an adiabatic lower horizontal wall and an upper isothermal wall. With such boundary conditions, no external thermal forcing is prescribed, and the temperature gradient of the basic flow is only a consequence of the flow rate, through the volumetric heating induced by viscous dissipation.

Barletta & Nield (2010) proved that the longitudinal rolls superposed to the PCF are the most unstable normal modes. These authors showed that the order parameter for the onset of convective instability is given by the product $Ge\,Pe^2$, where Ge is the Gebhart number and Pe is the Péclet number. The critical value of $Ge\,Pe^2$ is given by 2772.27 Barletta & Nield (2010). A similar analysis of the PPF was developed by Barletta *et al.* (2011). Also in this case, the longitudinal rolls turned out to be the most unstable normal modes with a critical value of $Ge\,Pe^2$ given by 221.2619. More precisely, those critical values of $Ge\,Pe^2$ were evaluated in both cases by assuming an infinitely large Prandtl number, Pr. This limit is a sensible one given that the sole cause of the instability is the viscous dissipation. In fact, Barletta *et al.* (2011) proved that the critical value of $Ge\,Pe^2$ decreases with Pr and attains its minimum when $Pr \to \infty$.

For instability induced by viscous dissipation, inertia is no longer the sole source of non-

linearity. Nonlinear thermal advection and nonlinear contribution of viscous dissipation interact in a nontrivial way even at low Re. Therefore the impact of these nonlinearities is examined in the framework of a weakly nonlinear stability analysis for the instability caused by viscous dissipation both in the PPF and PCF configurations. Our aim is to determine the nature of the bifurcation (supercritical/subcritical) and to report a quantitative analysis of the equilibrium disturbance amplitude and the average heat transfer beyond the bifurcation point.
The plan of this article is as follows. In section 2, the governing equations, the basic state and the formulation of its linear stability are presented. A weakly nonlinear analysis is performed in section 3 with the derivation of the amplitude equation. Results on the nature of bifurcations, the equilibrium amplitude of finite disturbances and the average heat transfer are presented in section 4. A conclusion is given in section 5.

2. Governing equations, basic state and dominant modal instability

Let us consider plane Poiseuille or plane Couette flow between two horizontal impermeable walls, which are set at a distance h apart. The upper wall is kept at a constant temperature T_1, while the lower wall is adiabatic. We Assume that the Oberbeck-Boussinesq approximation holds and we take into account viscous dissipation.
The governing equations are non-dimensionalized with the use of the following non-dimensional quantities:

$$(x, y, z) = \frac{(x^*, y^*, z^*)}{h},\ t = \frac{\kappa}{h^2}t^*,\ \mathbf{u} = \frac{h}{\kappa}\mathbf{u}^*,\ P = \frac{h^2}{\mu\kappa}P^*,\ T = \frac{(T^* - T_1)\beta g h}{\nu\kappa}$$

where $\mathbf{u}^* = (u^*, v^*, w^*)$, T^* and P^* are the dimensionless velocity vector, temperature and pressure, respectively. While κ is the thermal diffusivity, ρ_0 is the reference mass density, ν is the kinematic viscosity, μ is the dynamic viscosity, β is the thermal expansion coefficient of the fluid and g is the modulus of the gravitational acceleration, respectively. The dimensionless governing equations for continuity, momentum, and energy can be written as Barletta *et al.* (2011)

$$\boldsymbol{\nabla} \cdot \boldsymbol{u} = 0 \tag{2.1}$$

$$\frac{\partial \boldsymbol{u}}{\partial t} + (\boldsymbol{u} \cdot \boldsymbol{\nabla})\boldsymbol{u} = Pr\left(-\boldsymbol{\nabla} P - T\boldsymbol{e}_z + \boldsymbol{\nabla}^2 u\right) \tag{2.2}$$

$$\frac{\partial T}{\partial t} + \boldsymbol{u} \cdot \boldsymbol{\nabla} T = \boldsymbol{\nabla}^2 T + 2GeD_{ij}D_{ij} \tag{2.3}$$

where $D_{ij} = \frac{1}{2}(u_{i,j} + u_{j,i})$ is the strain tensor. The temperature boundary conditions can be expressed as

$$\frac{\partial T}{\partial z} = 0 \text{ at } z = 0 \quad \text{and} \quad T = 0 \text{ at } z = 1 \tag{2.4}$$

The velocity field boundary conditions for plane Poiseulle flow (PPF) are

$$\boldsymbol{u} = 0 \text{ at } z = 0; 1 \tag{2.5}$$

and for plane Couette flow (PCF)

$$\boldsymbol{u} = Pe\ \boldsymbol{e}_x \text{ at } z = 0 \quad \text{and} \quad \boldsymbol{u} = -Pe\ \boldsymbol{e}_x \text{ at } z = 1 \tag{2.6}$$

The three dimensionless parameters, appearing in the governing Eqs. (2.1)-(2.3) are the Prandtl number, the Péclet number, and the Gebhart number defined respectively by

$$Pr = \frac{\nu}{\kappa},\quad Pe = \frac{U_0 h}{\kappa},\quad Ge = \frac{\beta g h}{C}$$

where U_0 is the dimensional average velocity over the channel cross-section of Poiseuille flow and the modulus of the dimensional velocity of the moving upper ad lower plates in Couette flows and C is the specific heat of the fluid.
A basic stationary solution of (2.1)-(2.3) for the velocity and the temperature fields are given by

$$\boldsymbol{u}_b(z) = Pe\, f(z)\, \boldsymbol{e}_x \tag{2.7}$$

$$T_b(z) = Pe^2 Ge\, g(z) \tag{2.8}$$

with functions $f(z)$ and $g(z)$ being defined as

$$f(z) = 6z(1-z) \quad , \quad g(z) = 6(1 - 3z^2 + 4z^3 - 2z^4)$$

for Poiseuille flows, and

$$f(z) = z \quad , \quad g(z) = \frac{1}{2}(1 - z^2)$$

for Couette flows.
It can be noted from expression (2.8) that the base temperature is the result of the viscous dissipation, and vanishes in the absence of throughflow ($Pe = 0$). To investigate the stability of the above basic flow, an infinitesimal disturbance is superimposed to it,

$$\begin{cases} T = T_b(z) + \theta(x, y, z, t) \\ \boldsymbol{u} = \boldsymbol{u}_b(z) + \boldsymbol{U}(x, y, z, t) \\ P = P_b(x, z) + p(x, y, z, t) \end{cases} \tag{2.9}$$

The perturbation of the velocity field $\boldsymbol{U}$ has Cartesian components (u, v, w). The disturbances are developed in normal form modes,

$$\begin{cases} \boldsymbol{U} = \boldsymbol{U_n}(z) e^{ik_x x + ik_y y} e^{(\sigma + i\omega)t} \\ \theta = \theta_n(z) e^{ik_x x + ik_y y} e^{(\sigma + i\omega)t} \\ p = p_n(z) e^{ik_x x + ik_y y} e^{(\sigma + i\omega)t} \end{cases} \tag{2.10}$$

where $\boldsymbol{k} = k_x \boldsymbol{e}_x + k_y \boldsymbol{e}_y$ is the wave vector, σ is the temporal growth rate of the perturbation and ω is the frequency.
The linearized disturbance equations can be written as

$$i\, k_x\, u_n + i\, k_y\, v_n + \mathrm{D}w_n = 0 \tag{2.11}$$

$$\frac{1}{Pr}\left\{i\omega\, u_n + w_n\, Pe\, f'(z) + i\, k_x\, Pe\, f(z)\, u_n\right\} - (\mathrm{D}^2 - k^2)\, u_n + i\, k_x\, p_n = 0 \tag{2.12}$$

$$\frac{1}{Pr}\left\{i\omega\, v_n + i\, k_x\, Pe\, f(z)\, v_n\right\} - (\mathrm{D}^2 - k^2)\, v_n + i\, k_y\, p_n = 0 \tag{2.13}$$

$$\frac{1}{Pr}\left\{i\omega\, w_n + i\, k_x\, Pe\, f(z)\, w_n\right\} - (\mathrm{D}^2 - k^2)\, w_n + \mathrm{D}p_n - \theta_n = 0 \tag{2.14}$$

$$i\,\omega\,\theta_n + i\, k_x\, Pe\, f(z)\,\theta_n + Ge\, Pe^2\, g'(z)\, w_n - 2Ge\, Pe\, f'(z)\,(\mathrm{D}u_n + i\, k_x\, w_n) - (\mathrm{D}^2 - k^2)\,\theta_n = 0 \tag{2.15}$$

The boundary conditions for the disturbances are

$$\begin{cases} \mathrm{D}\theta_n = 0 \text{ at } z = 0 \text{ and } \theta_n = 0 \text{ at } z = 1 \\ u_n = w_n = \mathrm{D}w_n = 0 \text{ at } z = 0; 1 \end{cases} \tag{2.16}$$

Where D stands for d/dz.
These equations form a generalized eigenvalue problem that was recently solved by Barletta & Nield (2010) for PCF and by Barletta *et al.* (2011) for PPF. These authors determined the linear properties of disturbances in the form of longitudinal rolls, transverse rolls, and obliques rolls defined respectively by ($k_x = 0$, $k_y = k$), ($k_x = k$, $k_y = 0$) and ($k_x \neq 0$, $k_y \neq 0$). They found that stationary longitudinal rolls are the preferred mode of convection. They also showed that for the longitudinal rolls, apart from the wave number $k = k_y$, the only governing parameters are $\Lambda = Ge\,Pe^2$ and Pr, while neither Pe nor Ge appears explicitly. As a consequence, they computed the critical values Λ_c and k_c for different values of Pr, from which the system becomes unstable.
As longitudinal rolls are the dominant modes of convection induced by viscous dissipation instability, the present weakly nonlinear analysis is aimed to study their nonlinear dynamics above criticality.
Before considering the nonlinear problem, we emphasize that equation (2.12) written at the onset of stationary longitudinal rolls is reduced to

$$Re\, f'(z)\, w_n \;-\; (\mathrm{D}^2 - k^2)\, u_n = 0 \tag{2.17}$$

where $Re = Pe/Pr$ is the Reynolds number. If $Re = 0$, the solution to equation (2.17) satisfying boundary conditions is $u_n = 0$. For a non vanishing Reynolds number, the base flow shear $Re\, f'(z)$ transported by the vertical component of velocity will produce a u-velocity. This is why we will use the scaling $u = Re\,\tilde{u}$ in the following.

3. Weakly nonlinear analysis

3.1. *Governing equations for finite amplitude longitudinal rolls*

The governing equations of finite longitudinal rolls perturbations (i.e. $\partial/\partial x = 0$) in PPF/PCF are

$$\frac{\partial v}{\partial y} + \frac{\partial w}{\partial z} = 0 \tag{3.1}$$

$$\frac{1}{Pr}\frac{\partial \tilde{u}}{\partial t} + f'(z)w - \left(\frac{\partial^2}{\partial y^2} + \frac{\partial^2}{\partial z^2}\right)\tilde{u} = -\frac{1}{Pr}\left(v\frac{\partial \tilde{u}}{\partial y} + w\frac{\partial \tilde{u}}{\partial z}\right) \tag{3.2}$$

$$\frac{1}{Pr}\frac{\partial v}{\partial t} - \left(\frac{\partial^2}{\partial y^2} + \frac{\partial^2}{\partial z^2}\right)v + \frac{\partial P}{\partial y} = -\frac{1}{Pr}\left(v\frac{\partial v}{\partial y} + w\frac{\partial v}{\partial z}\right) \tag{3.3}$$

$$\frac{1}{Pr}\frac{\partial w}{\partial t} - \left(\frac{\partial^2}{\partial y^2} + \frac{\partial^2}{\partial z^2}\right)w - \theta + \frac{\partial P}{\partial z} = -\frac{1}{Pr}\left(v\frac{\partial w}{\partial y} + w\frac{\partial w}{\partial z}\right) \tag{3.4}$$

$$\begin{aligned}\frac{\partial \theta}{\partial t} + \Lambda g'(z)w - 2\frac{\Lambda}{Pr}f'(z)\frac{\partial \tilde{u}}{\partial z} - \left(\frac{\partial^2}{\partial y^2} + \frac{\partial^2}{\partial z^2}\right)\theta = \\ -\left(v\frac{\partial \theta}{\partial y} + w\frac{\partial \theta}{\partial z}\right) + Ge\left(\left(\frac{\partial v}{\partial z} + \frac{\partial w}{\partial y}\right)^2 + 4\left(\frac{\partial w}{\partial z}\right)^2\right) + \\ \frac{\Lambda}{Pr^2}\left(\left(\frac{\partial \tilde{u}}{\partial y}\right)^2 + \left(\frac{\partial \tilde{u}}{\partial z}\right)^2\right)\end{aligned} \tag{3.5}$$

We note that the equations (3.2)-(3.5) greatly simplified for a special case of fluids with $Pr \gg 1$, i.e. the momentum diffusivity dominates the viscous diffusivity. In particular, the terms involving the $\tilde{u}$-derivatives disappear from equation (3.5) in this limit and consequently linear and nonlinear stability analysis may be conducted without referring

to equation (3.2).
The pressure field is eliminated by cross-derivatives of (3.3) and (3.4) and substracting the obtained equations. Then the governing equations may be written in terms of reduced variables, namely, the stream function ψ defined by $-\partial\psi/\partial y = w$ and $\partial\psi/\partial z = v$, the temperature perturbation θ and the component $\tilde{u}$. The general governing equations for longitudinal rolls may be written in the compact notation

$$(\mathcal{L}^{'}\partial_t + \mathcal{L})\tilde{V} = N, \tag{3.6}$$

where the vector $\tilde{V} = (\psi, \theta, \tilde{u})^T$ and $N = \left(N_I^{\psi}, N_{Adv} + N_{Diss}^{Ge} + N_{Diss}^{Pr}, N_I^{\tilde{u}}\right)^T$.
The expressions of the linear operators $\mathcal{L}^{'}$ and $\mathcal{L}$ and the nonlinear contributions are the following:

$$\mathcal{L}^{'} = \begin{pmatrix} \frac{1}{Pr}\left(\frac{\partial^2}{\partial y^2} + \frac{\partial^2}{\partial z^2}\right) & 0 & 0 \\ 0 & 1 & 0 \\ 0 & 0 & \frac{1}{Pr} \end{pmatrix}, \tag{3.7}$$

$$\mathcal{L} = \begin{pmatrix} -\left(\frac{\partial^2}{\partial y^2} + \frac{\partial^2}{\partial z^2}\right)^2 & \frac{\partial}{\partial y} & 0 \\ -\Lambda g'(z)\frac{\partial}{\partial y} & -\left(\frac{\partial^2}{\partial y^2} + \frac{\partial^2}{\partial z^2}\right) & -2\frac{\Lambda}{Pr} f'(z)\frac{\partial}{\partial z} \\ -f'(z)\frac{\partial}{\partial y} & 0 & -\left(\frac{\partial^2}{\partial y^2} + \frac{\partial^2}{\partial z^2}\right) \end{pmatrix} \tag{3.8}$$

$$\begin{cases} N_I^{\psi} = \dfrac{1}{Pr}\left(\dfrac{\partial\psi}{\partial y}\dfrac{\partial}{\partial z} - \dfrac{\partial\psi}{\partial z}\dfrac{\partial}{\partial x}\right)\left(\dfrac{\partial^2}{\partial y^2} + \dfrac{\partial^2}{\partial z^2}\right)\psi \\ N_{Adv} = \dfrac{\partial\psi}{\partial y}\dfrac{\partial\theta}{\partial z} - \dfrac{\partial\psi}{\partial z}\dfrac{\partial\theta}{\partial y} \\ N_{Diss}^{Ge} = Ge\left[\left(\dfrac{\partial^2\psi}{\partial z^2} - \dfrac{\partial^2\psi}{\partial y^2}\right)^2 + 4\left(\dfrac{\partial^2\psi}{\partial y\partial z}\right)^2\right] \\ N_{Diss}^{Pr} = \dfrac{\Lambda}{Pr^2}\left[\left(\dfrac{\partial\tilde{u}}{\partial y}\right)^2 + \left(\dfrac{\partial\tilde{u}}{\partial z}\right)^2\right] \\ N_I^{\tilde{u}} = \dfrac{1}{Pr}\left[\dfrac{\partial\tilde{u}}{\partial z}\dfrac{\partial\psi}{\partial y} - \dfrac{\partial\tilde{u}}{\partial y}\dfrac{\partial\psi}{\partial z}\right] \end{cases} \tag{3.9}$$

The boundary conditions for the disturbances in PPF and PCF are

$$\begin{cases} \dfrac{\partial\theta}{\partial z} = 0 \text{ at } z = 0 \text{ and } \theta = 0 \text{ at } z = 1 \\ \tilde{u} = \psi = \dfrac{\partial\psi}{\partial z} = 0 \text{ at } z = 0; 1 \end{cases} \tag{3.10}$$

We note that in addition to the governing parameters Λ and Pr which appear in the linear operators $\mathcal{L}^{'}$ and $\mathcal{L}$, the nonlinear contribution of the term N_{Diss} introduces the Gebhart number Ge as a third dimensionless parameter.

3.2. *Derivation of amplitude equation*

Above the linear threshold, we introduce a small parameter ε which measures the distance to criticality by setting $\Lambda = \Lambda_c + \varepsilon^2 \Lambda_2$, where Λ_2 is of order unity. This fixes the temporal scaling to

$$t_2 = \varepsilon^2 t. \tag{3.11}$$

Temporal derivative is then replaced by

$$\frac{\partial}{\partial t} \rightarrow \frac{\partial}{\partial t} + \varepsilon^2 \frac{\partial}{\partial t_2}. \tag{3.12}$$

The evolution equations are obtained by expanding the vector $\tilde{V}$, the linear operator $\mathcal{L}$ and the nonlinear contribution N in power series of ε:

$$\begin{cases} \tilde{V} = \varepsilon \tilde{V}_1 + \varepsilon^2 \tilde{V}_2 + ... \\ \mathcal{L} = \mathcal{L}_c + \varepsilon^2 \Lambda_2 \mathcal{L}_2 + ... \\ N = \varepsilon^2 N_2 + \varepsilon^3 N_3 + ... \end{cases} \tag{3.13}$$

with the linear operator $\mathcal{L}_2$,

$$\mathcal{L}_2 = \begin{pmatrix} 0 & 0 & 0 \\ -g'(z)\frac{\partial}{\partial y} & 0 & -\frac{2}{Pr} f'(z)\frac{\partial}{\partial z} \\ 0 & 0 & 0 \end{pmatrix} \tag{3.14}$$

The vectors $\tilde{V}_i$ depend also on the slow variable t_2. By substituting the expressions (3.13) and (3.12) in the system (3.6), and then collecting coefficients of $O(\varepsilon)$, a set of equations is obtained.

3.2.1. *Eigenvalues and eigenfunctions at the first order problem*

To first order, the set of linear homogeneous equations for $\tilde{V}_1 = (\psi_1, \theta_1, \tilde{u}_1)^T$ at criticality is given by

$$\mathcal{L}_c \tilde{V}_1 = 0. \tag{3.15}$$

with $\mathcal{L}_c$ is the linear operator $\mathcal{L}$ for $\Lambda = \Lambda_c$. The solutions of Eq. (3.15) are developed in normal modes,

$$(\psi_1, \theta_1, \tilde{u}_1) = A(t_2) \left(\Psi_1(z), \Theta_1(z), \tilde{U}_1(z)\right) e^{ik_c y} + CC \tag{3.16}$$

where CC stands for a complex conjugate.
The boundary conditions for the eigenfunctions $\left(\Psi_1(z), \Theta_1(z), \tilde{U}_1(z)\right)$ are

$$\begin{cases} D\Theta_1 = 0 \text{ at } z = 0 \text{ and } \Theta_1 = 0 \text{ at } z = 1 \\ \tilde{U}_1 = \Psi_1 = D\Psi_1 = 0 \text{ at } z = 0; 1 \end{cases} \tag{3.17}$$

The eigenvalues of the problem, equations (3.15) and (3.16), with boundary conditions (3.17) are determined numerically with a shooting method. The accuracy and validity of the numerical scheme are checked by comparing our results with the published results of linear stability for PPF Barletta *et al.* (2011) at varying Prandtl numbers and PCF in the limit of infinite Pr considered in Barletta & Nield (2010). Table 1 presents the critical values Λ_c and the corresponding critical wavenumbers k_c for a wide range of Prandtl

	Present work (PPF)		Published work(PPF)		Present work (PCF)		Published work (PCF)	
Pr	Λ_c	k_c	Λ_c	k_c	Λ_c	k_c	Λ_c	k_c
∞	221.2619	2.572052	221.2619	2.572049	2772.27	2.62928	2772.27	2.62929
10^5	221.2621	2.572053	221.2621	2.572050	2772.2 8	2.62929	-	-
10^4	221.2638	2.572062	221.2638	2.572059	2772.33	2.62933	-	-
10^3	221.2807	2.572157	221.2807	2.572154	2772.85	2.62975	-	-
500	221.2994	2.572263	221.2994	2.572260	2773.43	2.63022	-	-
100	221.4493	2.573108	221.4493	2.573107	2778.06	2.63398	-	-
10	223.1388	2.582704	223.1388	2.582712	2830.54	2.67681	-	-
7	223.9452	2.587328	223.9452	2.587340	2855.78	2.69751	-	-
5	225.0221	2.593544	225.0221	2.593562	2889.65	2.72541	-	-
2	230.7001	2.62716	-	-	3071.61	2.87523	-	-
1	240.1912	2.686176	240.1912	2.686186	-	-	-	-
0.7	248.2572	2.738899	248.2572	2.738910	3680.61	3.33486	-	-
0.6	-	-	-	-	3851.73	3.44717	-	-
0.5	258.7369	2.810402	258.7369	2.810392	4106.72	3.60155	-	-
0.3	280.8701	2.968876	280.8701	2.968871	5455.16	4.24132	-	-
0.2	301.8653	3.123134	301.8653	3.123132	-	-	-	-
0.1	321.2322	3.292120	321.2323	3.292129	-	-	-	-

TABLE 1. Critical parameters Λ_c and k_c at the onset of longitudinal rolls for different Pr for PPF and PCF and comparison with the results of Barletta *et al.* (2011) and by Barletta & Nield (2010).

numbers. As can be seen from the Table 1, our results are in very good agreement with the numerical computations given by Barletta *et al.* (2011) and by Barletta & Nield (2010). The critical value Λ_c at the onset of convection decreases with increasing Pr for both PPF and PCF. The Prandtl number has therefore a destabilizing effect. We also note that the critical value Λ_c for a fixed value of Pr is more than ten times higher in PCF than in PPF.

We compute the eigenfunctions with a definite normalization of the vertical component of the velocity. The normalization is choosen in a manner such that $\int_0^1 |w_1|^2 \, dz = k_c^2 \int_0^1 |\Psi_1|^2 \, dz = 1$. For the sake of conciseness, the eigenfunctions in PCF are not displayed, as they present essentially the same qualitative behavior.

The dependence of the eigenfuctions on the vertical coordinate in PPF is shown in figure 1 for different Pr. Computations indicate that the eigenfunctions Θ_1 and $\tilde{U}_1$ are real-valued while Ψ_1 is a pure imaginary-valued. As it is shown in figure 1, $Im(\Psi_1)$ and $\tilde{U}_1$ are respectively nearly even and odd with respect to the midplane reflection symmetry, while the eigenfunction Θ_1 has asymetric profile as a consequence of the asymmetric prescribed thermal boundary conditions. We also note that in contrast to Ψ_1 and $\tilde{U}_1$, the influence of Pr on the vertical distribution of Θ_1 is significant. For instance, we observe that the value of Θ_1 at the lower boundary decreases with the decrease of Pr, and eventually changes sign for small Prandtl number. There is also a significant change in the vertical temperature gradient in the lower half plane when Prandtl number varies, in comparison with the nearly constant temperature gradient in the upper plane. Note that the influence of Pr is due to the presence of the forcing term $-2\frac{\Lambda}{Pr} f'(z) \frac{\partial \tilde{u}_1}{\partial z}$ in the linear energy equation.

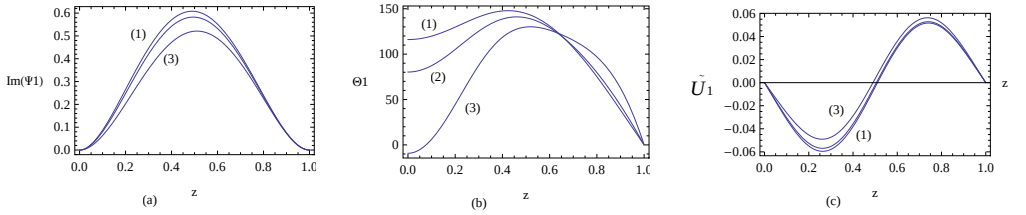

FIGURE 1. Eigenfunctions at critical conditions in PPF with different values of Prandtl number: (1) $Pr = 10^5$; (2) $Pr = 1$ and (3) $Pr = 0.27$.

3.2.2. *Solutions to the second order problem*

At $O(\varepsilon^2)$, the non homogenous problem for $\tilde{V}_2$ is given at criticality by,

$$\mathcal{L}_c \tilde{V}_2 \;=\; N_2(\tilde{V}_1), \tag{3.18}$$

The term N_2 at the right hand side of (3.18) is the nonlinear expression N evaluated to $O(\varepsilon^2)$. It contains known linear fundamental modes determined at $O(\varepsilon)$ $(\psi_1, \theta_1, \tilde{u}_1)$ and their derivatives. The nonlinear interactions between these fundamental modes and their complex conjugates generate higher harmonics and a modification of the basic state. The solutions to (3.18) are then sought in the form

$$(\psi_2, \theta_2, \tilde{u}_2) = \left[A(t_2)^2 \left(\Psi_{22}(z), \Theta_{22}(z), \tilde{U}_2(z)\right) e^{i2k_c y} + cc\right] + |A(t_2)|^2 \left(\Psi_{20}(z), \Theta_{20}(z), \tilde{U}_{20}(z)\right) \tag{3.19}$$

Substituting expressions (3.19) into equations (3.18), and separating the harmonic components, one obtains a system of equations for $\left(\Psi_{22}(z), \Theta_{22}(z), \tilde{U}_2(z)\right)$ and a system of equations for $\left(\Psi_{20}(z), \Theta_{20}(z), \tilde{U}_{20}(z)\right)$. The boudary conditions for $\left(\Psi_{22}(z), \Theta_{22}(z), \tilde{U}_2(z)\right)$ and $\left(\Psi_{20}(z), \Theta_{20}(z), \tilde{U}_{20}(z)\right)$ are the same as for $\tilde{V}_1$, equation (3.17).

As for the linear eigenfunctions, the nonlinear corrections are computed numerically. The properties of the nonlinear corrections at small and large Prandtl number are of interest. They are determined by different dominant nonlinearities defined by equation (3.9). For $Pr \gg 1$, the dominant nonlinear effect lies in advection of temperature (i.e. nonlinear terms N_{Adv}) and in a part of the viscous dissipitation (i.e. nonlinear terms N^{Ge}_{Diss}). While in the case of $Pr \ll 1$, advection of velocity prevails (i.e. nonlinear terms N^{ψ}_{I} and $N^{\tilde{u}}_{I}$) together with a part of the viscous dissipitation term (i.e. nonlinear terms N^{Pr}_{Diss}).

Independently of Prandtl number, numerical results indicate that

$$\Psi_{20}(z) = \tilde{U}_{20}(z) = 0 \tag{3.20}$$

Profiles of $Im(\Psi_{22}(z))$, $\tilde{U}_{22}(z)$, $\Theta_{22}(z)$ and $\Theta_{20}(z)$ are shown in figure 2 for $Pr = 10^5$ (curve (1)), $Pr = 1$ (curve (2)) and $Pr = 0.27$ (curve (3)). For $Pr = 10^5$, $Im(\Psi_{22}(z))$ and $\Theta_{22}(z)$ are positive for all z. By considering the expression of $\psi_{22}(z))$ and $\theta_{22}(z)$ given by (3.19), we can easily show that the effect of the first harmonics near the two vertical edges of a roll is to warm up and accelerate the upflow and to cool down and decelerate the downflow. On the other hand, for $Pr = 0.27$, $Im(\Psi_{22}(z))$ and $\Theta_{22}(z)$ are negative for all z

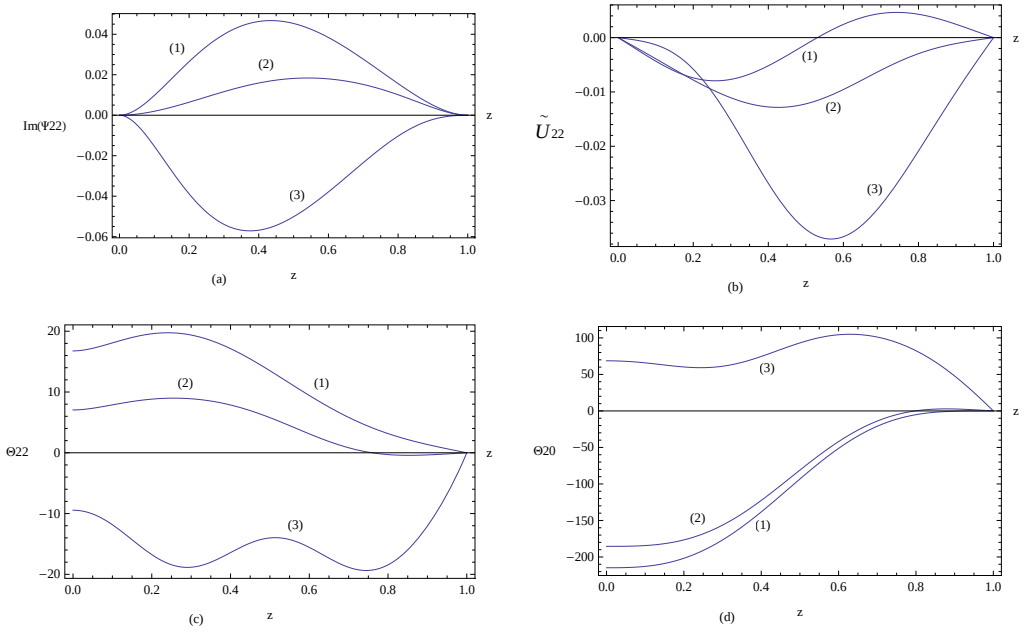

FIGURE 2. Vertical variations of the first nonlinear corrections to the linear mode at critical conditions in PPF with different values of Prandtl number: (1) $Pr = 10^5$; (2) $Pr = 1$ and (3) $Pr = 0.27$.

and the effect of the first harmonics is to cool down and to decelerate the warm upflow and to warm up and accelerate the cold downflow. As a consequence we can expect that the isolines of the stream function streche towards the warm upflow (the cold downflow) for $Pr = 10^5$ ($Pr = 0.27$) near the vertical edge of a roll. More importantly, the nonlinearities of the problem act to produce a temperature correction $\Theta_{20}(z)$ of the basic temperature distribution that strongly depends on the Prandtl number. For $Pr = 10^5$ and $Pr = 1$, we see from figure 2.d that this correction is negative with a positive temperature gradient except near the upper plate, while for $Pr = 0.27$ the correction becomes positive with a negative temperature gradient, except for a region near the center of the cell. A positive correction of the basic temperature gradient means that the first nonlinearities induce a stabilizing effect and one can expect a supercritical bifurcation in this case. In contrast, a negative correction of the basic temperature gradient leads to a destabilizing effect of the nonlinearities and therefore may be considered as a precursor to the emergence of a subcritical bifurcation. This is the reason why we plot, in figure 3, the vertical dependence of the nonlinear correction $\frac{d\Theta_{20}}{dz}$ to the basic temperature gradient for $Pr = 1$, $Pr = 0.27$ and $Pr = 0.15$ for PPF and $Pr = 2$, $Pr = 0.8$ and $Pr = 0.5$ for PCF. This figure shows clearly that the spatial region with a positive gradient of the correction to the basic temperature shrinks as the Prandtl number decreases and eventually disappears for small Pr. As we will see later, the sign change of the nonlinear correction $d\Theta_{20}/dz$ from positive to negative at small Pr announces the transition from supercritical to subcritical bifurcation.

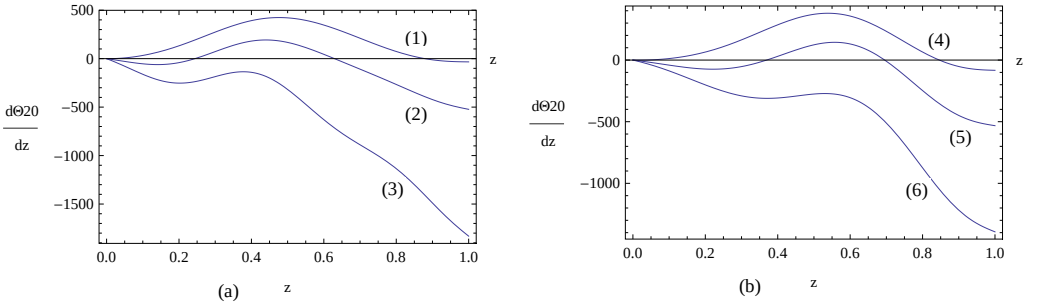

FIGURE 3. Correction of the basic temperature gradient $\frac{d\Theta_{20}}{dz}$ as a function of z: (a) PPF configuration (1) $Pr = 1$; (2) $Pr = 0.27$; (3) $Pr = 0.15$ and (b) PCF configuration (4) $Pr = 2$; (5) $Pr = 0.8$; (6) $Pr = 0.5$.

3.2.3. *Third order solvability condition*

At $O(\varepsilon^3)$, the following non homogenous problem for $\tilde{V}_3$ is obtained

$$\mathcal{L}_c \tilde{V}_3 = -(\mathcal{L}^{'} \partial_{t_2} + \Lambda_2 \mathcal{L}_2)\tilde{V}_1 + N_3(\tilde{V}_1, \tilde{V}_2), \tag{3.21}$$

The nonlinear term N_3 is the nonlinear expression N evaluated to $O(\varepsilon^3)$.
After inserting $\tilde{V}_1$ and $\tilde{V}_2$ into Eq. (3.21), there is no need to really solve this equation. Projecting instead the whole equation onto $\tilde{V}^{\dagger}$, where $\tilde{V}^{\dagger}$ is the solution to the adjoint of the linear problem yields a solvability condition, known as the Fredholm alternative. We Apply the solvability condition at $O(\varepsilon^3)$,

$$\langle -(\mathcal{L}^{'} \partial_{t_2} + \Lambda_2 \mathcal{L}_2)\tilde{V}_1 + N_3, \tilde{V}^{\dagger} \rangle = 0 \tag{3.22}$$

with the appropriate scalar product,

$$\left\langle \tilde{V}_i, \tilde{V}_j \right\rangle = \frac{1}{2\pi/k_c} \int_0^{2\pi/k_c} \int_0^1 \tilde{V}_i \cdot \tilde{V}_j^* dz\, dy, \tag{3.23}$$

where $\tilde{V}_j^*$ is the complex conjugate of $\tilde{V}_j$.
Re-introducing the original variables $t = t_2/\varepsilon^2$, $\Lambda_2 = (\Lambda - \Lambda_c)/\varepsilon^2$ and $A = \varepsilon A$ yields, the cubic Landau equation for the disturbance amplitude $A(t)$,

$$\tau \frac{\partial A}{\partial t} = \frac{\Lambda - \Lambda_c}{\Lambda_c} A - \lambda A|A|^2. \tag{3.24}$$

where

$$\tau = \frac{1}{\Lambda_c} \frac{\langle \mathcal{L}^{'} \partial_t \tilde{V}_1 , \tilde{V}^{\dagger} \rangle}{\langle \mathcal{L}_2 \tilde{V}_1, \tilde{V}^{\dagger} \rangle} \tag{3.25}$$

and

$$\lambda = -\frac{1}{\Lambda_c} \frac{\langle N_3 , \tilde{V}^{\dagger} \rangle}{\langle \mathcal{L}_2 \tilde{V}_1, \tilde{V}^{\dagger} \rangle} \tag{3.26}$$

Pr	λ (PPF)	τ (PPF)	λ (PCF)	τ (PCF)
∞	0.262305 - 0.0853848 Ge	0.0987665	0.251521 - 0.0794074 Ge	0.0920196
10^5	0.2623046 - 0.085384681 Ge	0.0987667	0.251521 - 0.0794071 Ge	0.0920195
100	0.262156 - 0.08531354 Ge	0.262158	0.25058 - 0.0790809 Ge	0.0918971
10	0.260701 - 0.08466750 Ge	0.260822	0.24392 - 0.0761753 Ge	0.0907209
7	0.2599332 - 0.08435667 Ge		0.240015 - 0.074817 Ge	0.0901216
5	0.258828 - 0.08393909 Ge	0.259312	0.234207 - 0.0730325 Ge	0.0892874
2	0.251571 - 0.0816911 Ge	0.105945	0.19294 - 0.0643027 Ge	0.0845216
1	0.23991 - 0.07778343 Ge	0.112204	-	-
0.77	-	-	0.004958 - 0.0473238 Ge	0.0718297
0.76	-	-	-0.000174 - 0.0470589 Ge	0.0715748
0.7	0.213541 - 0.06972831 Ge	0.117139	-0.03512 - 0.0454038 Ge	0.0699029
0.6	-	-	-0.114965 - 0.0424162 Ge	0.0663986
0.5	0.178989 - 0.06972831 Ge	0.123599	-0.240277 - 0.0392811 Ge	0.0613639
0.4	0.142607 - 0.06579806 Ge	0.129586	-0.457787 - 0.0365766 Ge	0.0527741
0.35	0.113554 - 0.0630992 Ge	0.134257	-	-
0.28	0.0491696 - 0.0581146 Ge	0.145108	-	-
0.27	0.036404 - 0.0572161 Ge	0.147275	-	-
0.25	0.0071595 - 0.0553392 Ge	0.152568	-	-
0.24	-0.00970435 - 0.0543286 Ge	0.155733	-	-
0.2	-0.097648 - 0.04975590 Ge	0.173631	-	-
0.15	-0.285401 - 0.0427067 Ge	0.219612	-	-
0.1	-0.681131 - 0.03422484 Ge	0.346653	-	-

TABLE 2. Coefficients λ and τ in Landau cubic equation for different Pr in PPF and PCF configurations.

4. Results of the weakly nonlinear stability

4.1. *Supercritical/subcritical bifurcation*

Computations of the characteristic time of instability τ and the first Landau constant λ indicate that they are real-valued. It is worth mentioning that the coefficient τ depends only on Pr whereas λ depends on Pr and Ge. In table 2 we give, for both PPF and PCF configurations, the numerical values of the characteristic time of instability τ as a function of Pr and the nonlinear coefficient λ as a function of Gebhart number for a very wide range of Pr. The coefficient τ is always positive independently of Pr while the nonlinear coefficient λ is positive or negative depending on Ge and Pr numbers. The sign of λ determines whether or not we are dealing with a subcritical bifurcation. The values of λ reported in table 2 indicate that independently of Gebhart number the bifurcation is subcritical (i.e. $\lambda < 0$) if $Pr < 0.25$ for PPF and if $Pr < 0.77$ for PCF. Otherwise, for higher Prandtl number, there exists a particular value of Gebhart number, Ge^* such that the bifurcation is supercrtical if $Ge < Ge^*$ or subcritical if $Ge > Ge^*$.

Figure 4 shows the variation of Ge^* as a function of Pr for PPF (line 1) and for PCF (line 2). As can be seen from this figure, variations of Ge^* become important only for $Pr < 1$, while for usual fluids with $Pr > 1$, Ge^* may be approximated by its asymptotic value $Ge^* = 3.072$ for PPF and $Ge^* = 3.167$ for PCF, obtained in the limit of infinite Prandtl number. As Gebhart number plays a key role in determining the supercritical or subcritical nature of the bifurcation, it is necessary to consider its realistic numerical values. From the physical point of view, high values of Ge can occur only in geophysical or in atmospheric flows, so one can expect the occurence of subcritical bifurcation for

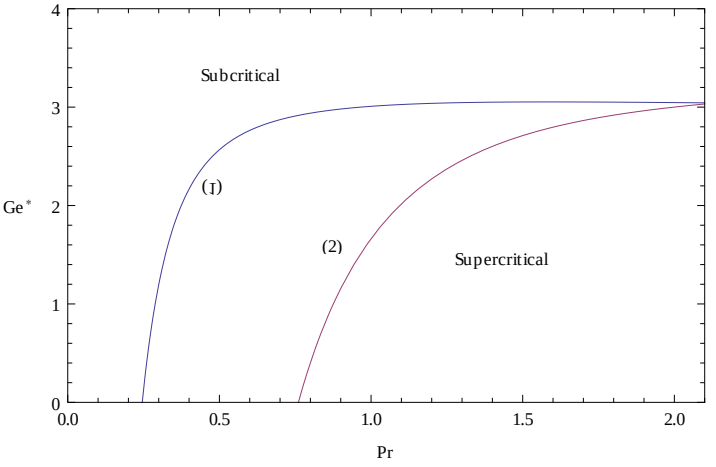

FIGURE 4. Dependence on Prandtl number of critical values Ge^* of the Gebhart number above which the bifurcation becomes subcritical.

such flows for both small and large Prandtl numbers. In contrast to these flows, and as pointed out in Barletta *et al.* (2011), if the fluid flow is on a typical laboratory scale, then Ge can hardly be greater than 10^{-5}. In this case a subcritical bifurcation is therefore restricted only to fluids with small Prandtl numbers.

To shed more light on the mechanism of supercritical/subcritical instability, an investigation of the effect on the first Landau constant of each of the three different nonlinear contributions present in the current problem is made. The nonlinear terms defined by equations (3.9) are $N_I = (N_I^{\psi}, 0, N_I^{\tilde{u}})^T$, $N_A = (0, N_{Adv}, 0)^T$ and $N_D = (0, N_{Diss}^{Ge} + N_{Diss}^{Pr}, 0)^T$ and represent respectively, nonlinear inertial terms, nonlinear thermal advection terms and terms modelling the nonlinear contribution of viscous dissipation.

The Landau constant may be written as the sum of three constants,

$$\lambda = \lambda_I + \lambda_A + \lambda_D \tag{4.1}$$

where

$$(\lambda_I\,, \lambda_A\,, \lambda_D) = -\frac{1}{\Lambda_c \langle\, \mathcal{L}_2 \tilde{V}_1, \tilde{V}^{\dagger}\rangle} \left(\langle N_I\,, \tilde{V}^{\dagger}\rangle, \langle N_A\,, \tilde{V}^{\dagger}\rangle, \langle N_D\,, \tilde{V}^{\dagger}\rangle\right) \tag{4.2}$$

The different contributions λ_I, λ_A, and λ_D to the Landau constant λ are determined by the computation of the integrals (4.2) at critical conditions (Λ_c, k_c) for different values of Ge and Pr.

We found that λ_I is zero independently of Ge and Pr, meaning that the inertial terms have no influence on the nonlinear evolution of the disturbance amplitude $A(t)$. On the other hand, we found that λ_A is the sum of two coefficients,

$$\lambda_A = \lambda_{Adv} + \lambda_A^D \tag{4.3}$$

The coefficient λ_{Adv} is due to thermal advection term if the nonlinear viscous dissipative term is ignored (i.e. $\lambda_{Adv} = \lambda_A(N_D = 0)$), while the thermal advection coefficient λ_A^D is strictly due to the presence of the nonlinear viscous dissipative term N_D. As a consequence, it is natural to define a new parameter λ_{vd} which measures the total contribution of the nonlinear viscous dissipative term,

$$\lambda_{vd} = \lambda_A^D + \lambda_D \tag{4.4}$$

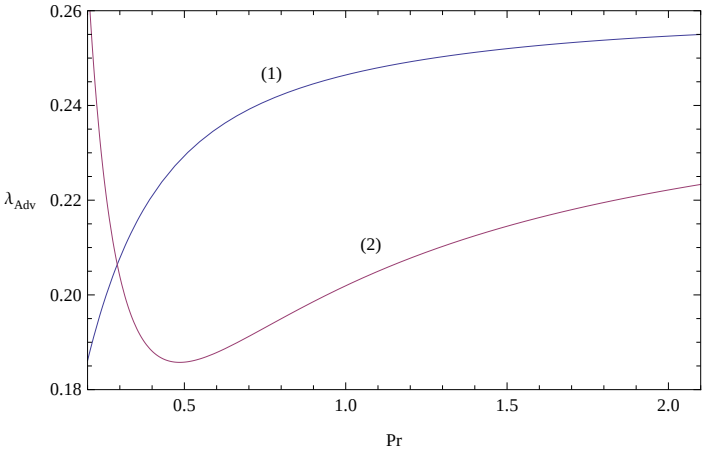

FIGURE 5. Dependence on Prandtl number of the coefficient λ_{Adv}.

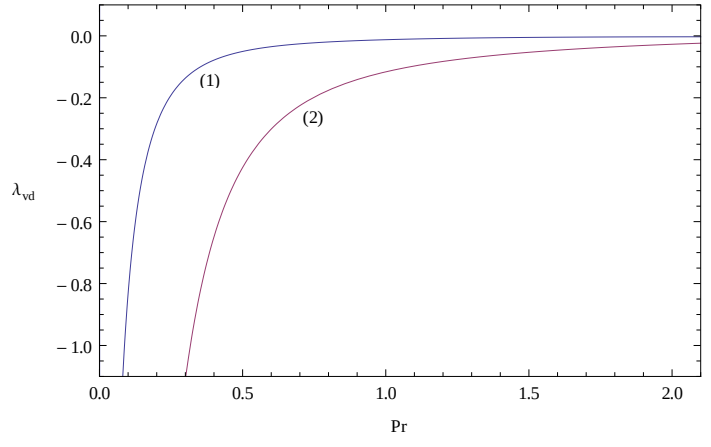

FIGURE 6. Dependence on Prandtl number of the coefficient λ_{vd} for $Ge = 10^{-4}$.

Equation (4.1) is then written as,

$$\lambda = \lambda_{Adv} + \lambda_{vd} \tag{4.5}$$

In figure 5, λ_{Adv} is plotted as a function of Pr for PPF (curve(1)) and for PCF (curve (2)). For both configurations, λ_{Adv} is positive meaning that the effect of nonlinear thermal advection terms is to promote supercritical bifurcation.
In figure 6 the dependencies of λ_{vd} on Pr for $Ge = 10^{-4}$ are plotted for PPF (curve (1)) and PCF (curve (2)). As can be observed, λ_{vd} is negative for both configurations regardless of Prandtl number. Therefore we conclude that the nonlinear terms N_D associated to the viscous dissipation promote a subcritical bifurcation. Computations of λ_{vd} with different Gehbart numbers lead qualitatively to the same result.

4.2. *Stationary amplitudes in the range of validity of the weakly nonlinear analysis*

The range of validity of the weakly nonlinear analysis based on the cubic amplitude equation (3.24) has to be discussed. The rigorous derivation of such equation requires the theoretical assumption that the bifurcation parameter Λ is near its critical value Λ_c at the onset of convection (i.e. $\epsilon \ll 1$). In practical applications of the weakly nonlinear

analysis, the range of validity of amplitude equations depends on the physical system under consideration. In a recent paper dealing with finite amplitude convection and heat transfer in inclined porous layer, Ouarzazi *et al.* (2017) derived a Landau equation by using a weakly nonlinear analysis. Comparing the theoretical predictions of Nusselt number with data from experiments, they found unexpectedly a very large range of validity of the derived amplitude equation, i.e. $\epsilon^2 = 2$ with ϵ measures the distance to the critical Darcy-Rayleigh number. On the other hand, Generalis & Fujimura (2009) examined the range of validity of amplitude equations in the context of Rayleigh-Bénard problem. They carried out fully numerical analysis on bifurcation of steady solutions for various Prandtl numbers. Comparing two results, they showed that the amplitude equation has a wide range of validity for Prandtl number larger than $O(1)$. For fluids with small Prandtl numbers, on the other hand, they showed a very narrow range of validity.

In order to assess the validity of the current weakly nonlinear analysis, we use the argument made by Métivier *et al.* (2010) in their investigation of thermoconvective instability involving viscoplastic fluids. This argument states that the necessary condition allowing the validity of the asymptotic expansion (3.13) may be written with our notation as,

$$|A| \ll |A_{Max}| \; = \; \frac{Max\,(|\tilde{V}_1|)}{Max\,(|\tilde{V}_2|)} \tag{4.6}$$

We observe from numerical results shown in figures 1 and 2 for PPF that $Max\,(|\tilde{V}_1|) = Max\,(|\Theta_1(z)|)$ and $Max\,(|\tilde{V}_2|) = Max\,(|\Theta_{20}(z)|)$ for the three fixed values of Prandtl number. The condition (4.6) implies $|A_{Max}| = 0.69\,;\ 0.76\,;\ 1.86$ respectively for $Pr = 10^5\,;\ Pr = 1\,;\ Pr = 0.27$. In the same manner, for PCF we found that $|A_{Max}| = 0.68\,;\ 0.95\,;\ 1.74$ respectively for $Pr = 10^5\,;\ Pr = 2\,;\ Pr = 0.77$.

The amplitude equation (3.24) predicts supercritical instability if the Landau constant λ is positive, with a stable stationary nonlinear equilibrium solution,

$$|A_s| \; = \; \left| \frac{\Lambda \, - \, \Lambda_c}{\lambda \Lambda_c} \right|^{1/2}, \tag{4.7}$$

If λ is negative, a subcritical instability is predicted with the threshold amplitudes $|A_s|$, which limit the basin of attraction of the linearly stable PPF and PCF flows for $\Lambda < \Lambda_c$. In that case, the cubic amplitude equation (3.24) does not provide any stable finite-amplitude equilibrium and therefore it is necessary to carry the analysis to higher orders in amplitude. This task is out of the scope of the present work.

Figure 7 presents the bifurcation diagrams for different Prandtl numbers showing the equilibrium amplitudes (up to $|A_s| = 0.1 << |A_{Max}|$) when the bifurcations are supercritical (continuous lines) and the threshold amplitudes (dashed lines) when the bifurcations are subcritical. The magnitude of $|A_s|$ for fixed values of $\frac{\Lambda - \Lambda_c}{\Lambda_c}$ decreases on increasing the value of Pr in the case of supercritical bifurcations. While for subcritical bifurcations, the bifurcation diagrams indicate that the thresold amplitudes decreases with the decrease of Pr, meaning that the basic PPF and PCF flows become strongly sensitive to finite amplitude perturbations when Pr is decreased.

4.3. *Heat transfer*

The conductive state supports a non-uniform heat flux $J_{cond}(z) = -\frac{dT_b}{dz}$ flowing vertically through the layer. The expression of the basic temperature $T_b(z)$ is given by (2.8). In the presence of a convective velocity field, the total stationary vertical flux is

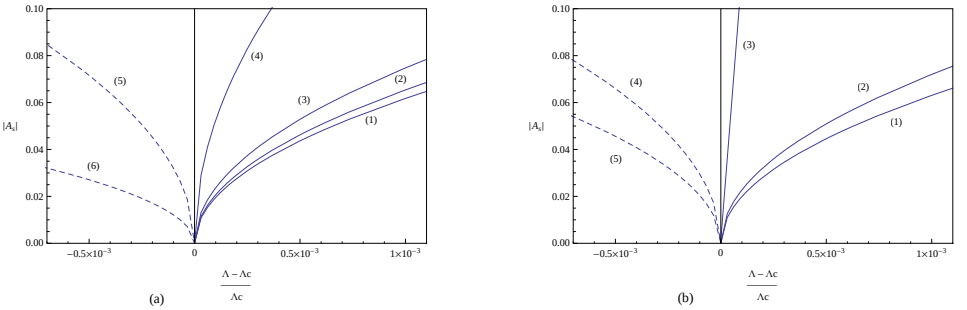

FIGURE 7. Stationary amplitude as a function of the distance to criticality: (a) PPF configuration (1) $Pr = 10^5$; (2) $Pr = 1$; (3) $Pr = 0.5$; (4) $Pr = 0.27$; (5) $Pr = 0.2$; (6) $Pr = 0.1$ and (b) PCF configuration (1) $Pr = 10^5$, (2) $Pr = 2$, (3) $Pr = 0.77$; (4) $Pr = 0.6$; (5) $Pr = 0.5$.

$J = J_{cond}(z) + J_{conv}(y, z)$, where J_{conv} is independent of x for longitudinal rolls with axes along the x direction and it reads

$$J_{conv}(y, z) = -\frac{\partial \psi}{\partial y}(T_b + \theta) - \frac{d\theta}{dz}. \tag{4.8}$$

The contribution $-\frac{\partial \psi}{\partial y}(T_b+\theta)$ to the convective flux J_{conv} describes convective transport of heat by the velocity field. The term $-\frac{d\theta}{dz}$ is the diffusive flux of heat, driven by the gradient in the convection-generated deviations of the temperature field from the conduction profile.
We define the lateral average convective heat flux by

$$\langle J_{conv}\rangle(z) = \frac{1}{2\pi/k_c}\int_0^{2\pi/k_c} J_{conv}(y, z)dy \tag{4.9}$$

We remark that owing to the boundary conditions (3.10) imposed at $z = 0$ and $z = 1$, $J_{conv}(z = 0) = 0$ and $J_{conv}(z = 1) = -\frac{d\theta}{dz}(z = 1)$. This means that the average heat flux $\langle J_{conv}\rangle(z)$ is z dependent and it is therefore instructive to investigate its vertical distribution in the fluid layer.
Figures (8) and (9) show typical plots of the vertical variations of the average heat flux $\langle J_{conv}\rangle(z)$ for (a) PPF and (b) PCF at $\Lambda = 1.1\Lambda_c$, $Ge = 10^{-4}$ and various Prandtl numbers corresponding to supercritical bifurcations. Figure (8) shows results for some high or moderate Prandtl numbers while figure (9) focuses on the regime of small Prandtl numbers. The average heat flux is found some orders of magnitude smaller at high Prandtl numbers than at small ones. On the other hand, the average heat flux exhibits a maximum located near the middle of the fluid layer at high Prandtl numbers. As the Prandtl number decreases, this maximum moves to the top and evenually reach the upper boundary.
Our aim now is to find the relation between the total heat flux and the heat flux in the conductive regime, transferred to the upper boundary. The relative contributions of conduction and convection on heat transferred to the upper plate is expressed using dimensionless Nusselt number Nu defined by

$$Nu(z = 1) = 1 + \frac{\langle J_{conv}(z = 1)\rangle}{J_{cond}(z = 1)} \tag{4.10}$$

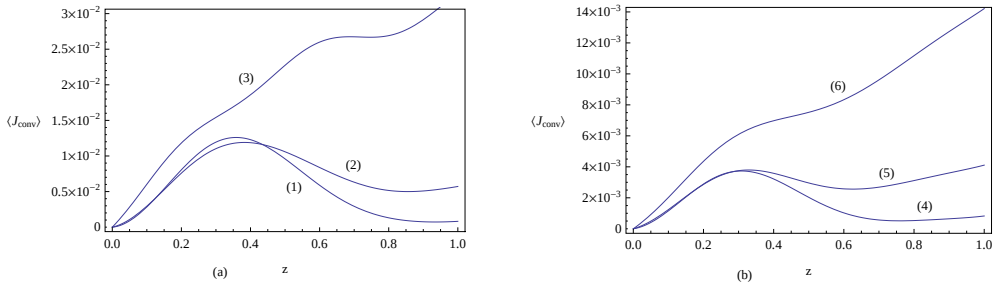

FIGURE 8. Vertical distribution of average convective heat flux at $\frac{\Lambda-\Lambda_c}{\Lambda_c}=10^{-3}$ for fluids with moderate and high Prandtl number: (a) PPF configuration (1) $Pr=10^5$; (2) $Pr=5$ and (3) $Pr=2$ and (b) for PCF configuration (4) $Pr=10^5$, (5) $Pr=20$, (6) $Pr=10$.

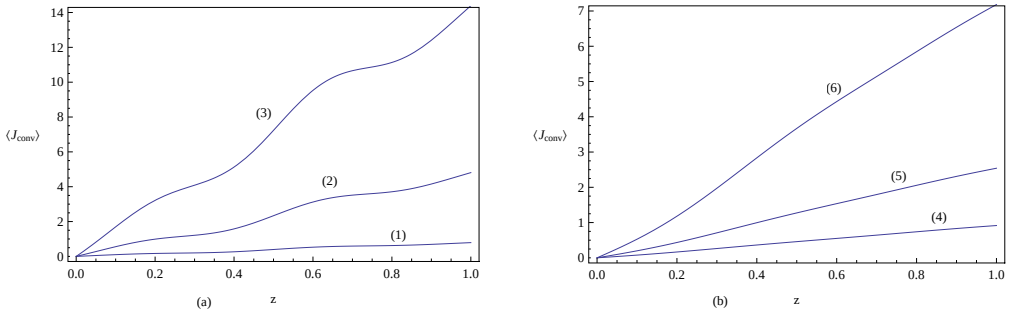

FIGURE 9. Vertical distribution of average convective heat flux at $\frac{\Lambda-\Lambda_c}{\Lambda_c}=10^{-3}$ for fluids with small Prandtl number: (a) PPF configuration (1) $Pr=0.5$, (2) $Pr=0.31$, (3) $Pr=0.27$ and (b) PCF configuration (4) $Pr=1.5$, (5) $Pr=1.1$, (6) $Pr=0.9$.

which may be written as

$$Nu=1-\frac{1}{12\Lambda}|A_s|^2\frac{d\Theta_{20}}{dz}|_{z=1} \qquad \text{for PPF} \tag{4.11}$$

$$Nu=1-\frac{1}{\Lambda}|A_s|^2\frac{d\Theta_{20}}{dz}|_{z=1} \qquad \text{for PCF} \tag{4.12}$$

According to figure 3, we notice that $\frac{d\Theta_{20}}{dz}|_{z=1}$ is negative and its absolute value decreases with increasing Prandtl number. The same trend is observed in the plots of $|A_s|$ shown in figure 7. Consequently, the Nusselt number evaluated at the upper plate decreases with increasing Prandtl number. Substituting the solution of $|A_s|$ given by (4.7) into (4.11) and (4.12) yields the following relationships

$$Nu=1-\frac{1}{12\lambda\Lambda_c}\frac{d\Theta_{20}}{dz}|_{z=1}\left(\frac{\Lambda-\Lambda_c}{\Lambda}\right) \qquad \text{for PPF} \tag{4.13}$$

$$Nu=1-\frac{1}{\lambda\Lambda_c}\frac{d\Theta_{20}}{dz}|_{z=1}\left(\frac{\Lambda-\Lambda_c}{\Lambda}\right) \qquad \text{for PCF} \tag{4.14}$$

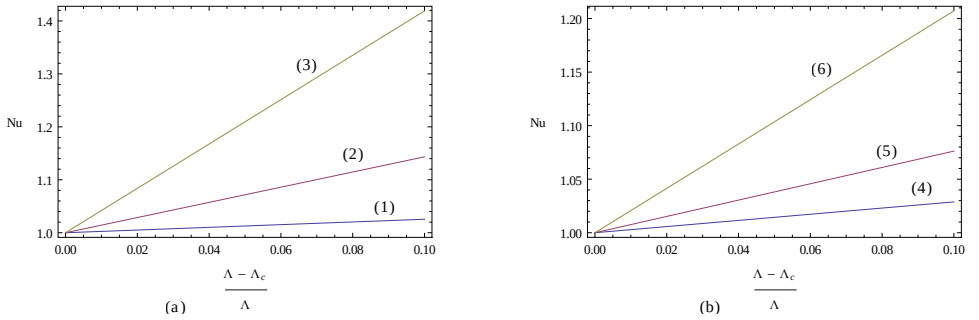

FIGURE 10. Nusselt number in the regime of small Prandtl numbers: (a) PPF configuration (1) $Pr = 0.5$, (2) $Pr = 0.31$, (3) $Pr = 0.27$ and (b) PCF configuration (4) $Pr = 1.5$, (5) $Pr = 1.1$, (6) $Pr = 0.9$

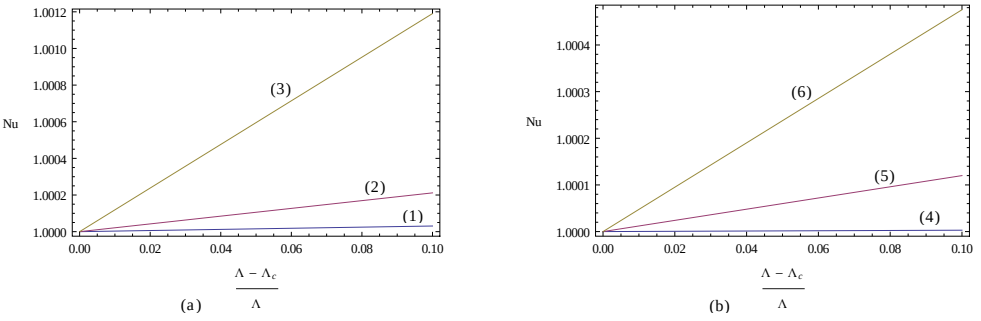

FIGURE 11. Nusselt number in the regime of moderate and high Prandtl numbers: (a) PPF configuration (1) $Pr = 10^5$; (2) $Pr = 5$ and (3) $Pr = 2$ and (b) PCF configuration (4) $Pr = 10^5$, (5) $Pr = 20$, (6) $Pr = 10$.

The variation of Nusselt number at the upper plate for PPF and PCF as a function of $\frac{\Lambda - \Lambda_c}{\Lambda}$ is shown in figure 10 for some small Prandtl numbers and in figure 11 for moderate to high values of Prandtl. Comparing the two figures we remark, as expected, that the slopes of Nusselt number $S = -\frac{1}{12\lambda\Lambda_c}\frac{d\Theta_{20}}{dz}|_{z=1}$ for PPF and $S = -\frac{1}{\lambda\Lambda_c}\frac{d\Theta_{20}}{dz}|_{z=1}$ for PCF decrease drastically with the increase of Prandtl number.

5. Conclusions

A linear and weakly nonlinear stability analysis of mixed convection in a plane parallel channel has been carried out. Both the basic solutions of Couette and Poiseuille flow have been considered. The effect causing the unstable thermal stratification and, as a consequence, the emergence of convection cells is the viscous dissipation. This effect is the sole cause of the vertical temperature gradient in the basic state, as no thermal forcing is imposed through the boundary walls. In fact, the lower wall has been assumed to be thermally insulated, while the upper wall is considered as isothermal.

The linear analysis has been surveyed relying on the previous studies by Barletta & Nield (2010) and Barletta *et al.* (2011). The results presented by these authors have been recovered and extended. The important result that the critical condition for the onset of

convective instability is triggered by longitudinal rolls has been highlighted as the basis for the weakly nonlinear analysis.

The study of the nonlinear behaviour has been carried out within the weakly nonlinear theory. We numerically obtained the linear fundamental modes and showed that their nonlinear interaction generates a modification of the basic temperature gradient. The effect of Prandtl number, Pr, on the correction of the basic temperature gradient induced by the first nonlinearities is examined. It emerges that this correction is globally positive for high and moderate Pr, while it becomes negative for all vertical position of the medium for small Pr. Physically, a negative modification of the basic temperature gradient discloses a destabilizing effect of the first nonlinearities and may be regarded as a signature of the presence of a subcritical bifurcation. The coefficients of the appropriate cubic Landau amplitude equation which describes stationary convection patterns beyond instability threshold have been computed for longitudinal rolls. The main results obtained through this analysis are the following:

• There exists a threshold value, Ge^*, of the Gebhart number, Ge, such that a supercritical bifurcation happens when $Ge < Ge^*$, while the bifurcation is subcritical for $Ge > Ge^*$. The value of Ge^* depends on Pr, both for the Couette and the Poiseuille flow.

• The effects of the three nonlinear terms in the governing equations, inertia, advection and viscous dissipation, have been discerned. The inertia term turned out to be ineffective as its contribution to the Landau constant is zero. The advection term tends to favour a supercritical bifurcation, while the dissipation term promotes a subcritical bifurcation.

• The heat transfer mechanism has been investigated in the case of a supercritical bifurcation by evaluating both the lateral average convective heat flux and the Nusselt number. The maximum average heat flux is found to be located near the middle of the fluid layer at high Pr while this maximum occurs at the upper boundary for small Pr. As a consequence, the Nusselt number evaluated at the upper boundary is reduced with the increase of Pr.

In this paper, we showed that for realistic values of the Gebhart number a high viscous dissipation effect reduces the subcritical character of the bifurcation, which may become supercritical for fluids with large Pr. However, it would be desirable to go beyond the cubic Landau amplitude equation by considering higher nonlinearities in order to compute the equilibrium amplitude for fluids with small Pr which yield a subcritical bifurcation. This task will be the objective of a future paper.

REFERENCES

de B. Alves, L. S., Hirata, S. C. & Ouarzazi, M. N. 2016 Linear onset of convective instability for rayleigh-bnard-couette flows of viscoelastic fluids. *Journal of Non-Newtonian Fluid Mechanics* **231**, 7990.

Barletta, A. 2015 On the thermal instability induced by viscous dissipation. *International Journal of Thermal Sciences* **88**, 238–247.

Barletta, A., Celli, M. & Nield, D. A. 2011 On the onset of dissipation thermal instability for the poiseuille flow of a highly viscous fluid in a horizontal channel. *Journal of Fluid Mechanics* **681**, 499–514.

Barletta, A. & Nield, D. A. 2010 Convection-dissipation instability in the horizontal plane couette flow of a highly viscous fluid. *Journal of Fluid Mechanics* **662**, 475–492.

Biau, D. & Bottaro, A. 2004 The effect of stable thermal stratification on shear flow instability. *Physics of Fluids* **16(14)**, 47424745.

Carrière, P. & Monkewitz, P. A. 1999 Convective versus absolute instability in mixed Rayleigh-Bénard-Poiseuille convection. *Journal of Fluid Mechanics* **384**, 243–262.

D. Martinand, P. Carrière & Monkewitz, P. A. 2006 Three-dimensional global instability

modes associated with a localized hot spot in rayleigh-bénard-poiseuille convection. *Journal of Fluid Mechanics* **551**, 275–301.

Dauchot, O. & Daviaud, F. 1995 Finite amplitude perturbation and spots growth mechanism in plane couette flow. *Journal of Fluid Mechanics* **7**, 335.

Generalis, S. C. & Fujimura, K. 2009 Range of validity of weakly nonlinear theory in the Rayleigh-Bénard problem. *J. Phys. Soc. Jpn* **78**, 8–084401.

Hirata, S. C., de B. Alves, L. S., Delenda, N. & Ouarzazi, M. N. 2015 Convective and absolute instabilities in rayleigh-bnard-poiseuille mixed convection for viscoelastic fluids. *Journal of Fluid Mechanics* **765**, 167210.

Hu, J., Ben Hadid, H. & Henry, D. 2007 Linear stability analysis of poiseuille-rayleigh-bénard flows in binary fluids with soret effect. *Physics of Fluids* **19**, 034101(1)–034101(17.

Jerome, JJS., Chomaz, J.-M. & Huerre, P. 2012 Transient growth in rayleigh-benard-poiseuille/couette convection. *Physics of Fluids* **24**, 044103.

Métivier, C., Nouar, C. & Brancher, J.-P. 2010 Weakly nonlinear dynamics of thermoconvective instability involving viscoplastic fluids. *Journal of Fluid Mechanics* **660**, 316–353.

Nicolas, X. 2002 Bibliographical review on the poiseuille-rayleigh-bénard flows: The mixed convection flows in horizontal rectangular ducts heated from below. *International Journal of Thermal Sciences* **41** (10), 961–1016.

Nishioka, M. & Asai, M. 1985 Some observations of the subcritical transition in plane poiseuille flow. *Journal of Fluid Mechanics* **150**, 441–450.

Nishioka, M., Iida, A. S. & Ichikawa, Y. 1975 An experimental investigation of the stability of plane poiseuille flow. *Journal of Fluid Mechanics* **72**, 731–751.

Orszag, S. A. 1971 Accurate solution of the orr-sommerfeld stability equation. *Journal of Fluid Mechanics* **50**, 689–703.

Orszag, S. A. & Patera, A. T. 1980 Subcritical transition to turbulence in plane channel flows. *Phys. Rev. Lett.* **45**, 989–993.

Ouarzazi, M. N., Hirata, S. C., Barletta, A. & Celli, M. 2017 Finite amplitude convection and heat transfer in inclined porous layer using a thermal non-equilibrium model. *International Journal of Heat and Mass Transfer* **113**, 399–410.

Ouarzazi, M. N., Mejni, F., Delache, A. & Labrosse, G. 2008 Nonlinear global modes in inhomogeneous mixed convection flows in porous media. *Journal of Fluid Mechanics* **595**, 367–377.

Romanov, V. 1973 Stability of plane-parallel couette flow. *Funct. Anal. Appl.* **7**, 137–146.

Tillmarki, N. & Alfredsson, P. 1992 Experiments on transition in plane couette flow. *Journal of Fluid Mechanics* **235**, 89–102.